ISSN 0018-151X, High Temperature, 2008, Vol. 46, No. 5, pp. 630–638. © Pleiades Publishing, Ltd., 2008.
Original Russian Text © K.N. Volkov, 2008, published in Teplofizika Vysokikh Temperatur, Vol. 46, No. 5, 2008, pp. 690–699.

HEAT AND MASS TRANSFER AND PHYSICAL GASDYNAMICS

Large Eddy Simulation of a Nonisothermal Turbulent Jet Flowing out into Submerged Space

K. N. Volkov

University of Surrey, Guilford, United Kingdom

Received April 13, 2007

Abstract—Large eddy simulation is performed of a subsonic nonisothermal turbulent jet flowing out from a round nozzle into submerged space. The Navier–Stokes equations filtered over space and the RNG model of subgrid-scale viscosity are used for describing the flow. The calculations are performed for different values of the degree of jet preheating. The processing of the results of numerical simulation enables one to obtain the distributions of correlation moments of fluctuations of density, velocity, and temperature along the axis and in cross sections of jet flow. The calculation results are compared with the available data obtained using the solution of Reynolds-averaged Navier–Stokes equations and equations of the k–ε model of turbulence, as well as with the data of physical experiment.

PACS numbers: 51.20.+d

DOI: 10.1134/S0018151X08050076

INTRODUCTION

Considerable attention is given in the literature to physical and mathematical simulation of subsonic turbulent jets.

The characteristics of nonisothermal jets were measured in [1–9]; main attention in [6–9] was given to the investigation of the degree of preheating on the turbulent structure of jet flow.

Various models of turbulence are employed for numerical calculations [10, 11], as well as present-day approaches to simulation of turbulence [12–18] such as direct numerical simulation (DNS) and large eddy simulation (LES). Referred to in [12] as direct numerical simulation were approaches in which the eddy viscosity depends on the step of difference grid. Shur et al. [13] and Tucker [14] performed calculations on a coarse grid without using any subgrid-scale model, and the dissipative mechanism was introduced using difference scheme (monotonically integrated LES—MILES).

The solution obtained using DNS or LES carries more information compared to the solution of Reynolds equations: it contains information both on the characteristics of mean flow (fields of velocity, temperature, and pressure) and on the spectral characteristics, two-point moments, and higher-order moments.

The Smagorinsky model [15, 16] and the structure function model [17] (which is reduced to Smagorinsky model under certain conditions), as well as the dynamic model [18] and semi-scale model [15], are used as the subgrid-scale model. In [16], the emphasis was on the processes of formation of mixing layer in the initial region of the jet and of its development downstream, as well as on the impact made by the value of Smagorinsky coefficient on the characteristics of the jet. The discrepancy between the theoretical and experimental data is explained by the intermittency of flow and reverse transition of energy from small to large eddies [15] (unlike the scale model, the Smagorinsky model does not include the reverse transition of energy).

Some researchers, for example, Yan and Su [15], employed the axisymmetric formulation of the problem; this contradicts the ideology of large eddy simulation, which presumes the solution of unsteady-state three-dimensional equations.

In the present study, the results of large eddy simulation of a subsonic nonisothermal turbulent jet are used for obtaining the distributions of correlation moments of fluctuations of density, velocity, and temperature, including those of higher-order moments, as well as the distributions of turbulent Prandtl number and of the constant appearing in the formula for turbulent viscosity. The distributions are calculated along the axis and in cross sections of jet flow. The calculation results are compared with the available results of numerical simulation and with the data of physical experiment.

BASIC EQUATIONS

We will consider a turbulent jet of heated gas, which flows out from a round nozzle into submerged space. The origin of coordinates is located at the nozzle exit section. The positive reading of coordinate x is made in the direction of propagation of the jet. The radius of nozzle exit section r_a is taken as the characteristic scale for variables with the dimensionality of length; the

velocity u_a and temperature T_a of gas at the nozzle exit section are taken as the characteristic scales for variables with the dimensionality of velocity and temperature. The ambient temperature is T_∞. The flow in the jet is characterized by the preheat parameter $\varphi = T_a/T_\infty$ (for isothermal jet, $\varphi = 1$) and by the degree of turbulence at the nozzle exit section $\theta = u'/u_a$, where u' is the fluctuation component of velocity.

Equations in Conservative Variables

In Cartesian coordinates (x, y, z), the unsteady-state flow of viscous compressible gas is described by the equation

$$\frac{\partial \mathbf{Q}}{\partial t} + \frac{\partial \mathbf{F}_x}{\partial x} + \frac{\partial \mathbf{F}_y}{\partial y} + \frac{\partial \mathbf{F}_z}{\partial z} = 0. \quad (1)$$

Equation (1) is complemented by the equation of state for perfect gas

$$p = (\gamma - 1)\rho\left[e - \frac{1}{2}(v_x^2 + v_y^2 + v_z^2)\right].$$

The vector of conservative variables $\mathbf{Q}$ and flow vectors $\mathbf{F}_x$, $\mathbf{F}_y$, and $\mathbf{F}_z$ have the form

$$\mathbf{Q} = \begin{pmatrix} \rho \\ \rho v_x \\ \rho v_y \\ \rho v_z \\ \rho e \end{pmatrix},$$

$$\mathbf{F}_x = \begin{pmatrix} \rho v_x \\ \rho v_x v_x + p - \tau_{xx} \\ \rho v_x v_y - \tau_{xy} \\ \rho v_x v_z - \tau_{xz} \\ (\rho e + p) v_x - v_x \tau_{xx} - v_y \tau_{xy} - v_z \tau_{xz} + q_x \end{pmatrix},$$

$$\mathbf{F}_y = \begin{pmatrix} \rho v_y \\ \rho v_y v_x - \tau_{yx} \\ \rho v_y v_y + p - \tau_{yy} \\ \rho v_y v_z - \tau_{yz} \\ (\rho e + p) v_y - v_x \tau_{yx} - v_y \tau_{yy} - v_z \tau_{yz} + q_y \end{pmatrix},$$

$$\mathbf{F}_z = \begin{pmatrix} \rho v_z \\ \rho v_z v_x - \tau_{zx} \\ \rho v_z v_y - \tau_{zy} \\ \rho v_z v_z + p - \tau_{zz} \\ (\rho e + p) v_z - v_x \tau_{zx} - v_y \tau_{zy} - v_z \tau_{zz} + q_z \end{pmatrix}.$$

The components of the viscous stress tensor and the constituents of the heat flux vector are found from the relations

$$\tau_{ij} = \mu_e\left(\frac{\partial v_i}{\partial x_j} + \frac{\partial v_j}{\partial x_i} - \frac{2}{3}\frac{\partial v_k}{\partial x_k}\delta_{ij}\right), \quad q_i = -\lambda_e \frac{\partial T}{\partial x_i}.$$

Here, t is the time; x, y, and z are Cartesian coordinates; v_x, v_y, and v_z are components of velocity in the coordinate directions x, y, and z; ρ is the density; p is the pressure; e is the total energy per unit mass; T is the temperature; and γ is the specific-heat ratio.

Equation (1) formally coincides with unsteady-state Reynolds equations. The effective viscosity μ_e is represented as the sum of molecular viscosity and subgrid-scale eddy viscosity, and the effective thermal conductivity λ_e is expressed in terms of eddy viscosity and Prandtl number.

Cylindrical coordinates (x, r, θ) are used for preassigning the boundary conditions and for processing the calculation results instead of Cartesian coordinates (x, y, z). The radial and circumferential components of velocity are related to Cartesian components of velocity by the relations

$$v_r = \frac{v_y y + v_z z}{(y^2 + z^2)^{1/2}}, \quad v_\theta = \frac{v_z y - v_y z}{(y^2 + z^2)^{1/2}}.$$

In view of the symmetry of computational domain and boundary conditions, the time average value of circumferential velocity is zero.

Subgrid-Scale Model

In the model of subgrid-scale viscosity, which is based on the renormalized group (RNG) theory, the calculation of effective viscosity reduces to the solution of nonlinear algebraic equation [19]

$$\mu_e = \mu[1 + H(X - C)]^{1/3}, \quad X = \frac{\mu_s^2 \mu_e}{\mu^3},$$

where $H(X)$ is the Heaviside function and $C = 100$. The subgrid-scale viscosity is found from the relation

describing the Smagorinsky formula [20], but with a different value of constant factor

$$\mu_s = \rho(C_R\Delta)|S|^2,$$

where

$$|S| = (2S_{ij}S_{ij})^{1/2}, \quad S_{ij} = \frac{1}{2}\left(\frac{\partial v_i}{\partial x_j} + \frac{\partial v_j}{\partial x_i}\right).$$

The value of $C_R = 0.157$ is assigned to the model constant. At $X \gg C$, the Smagorinsky formula is derived with model coefficient $C_S = (2C_R)^{1/4}/(2\pi) = 0.119$.

In the fully turbulent region of flow, $\mu_e \gg \mu$; therefore, $\mu_e \approx \mu_s$, and the RNG model reduces to the Smagorinsky model [20]. In the weakly turbulent region, the argument of Heaviside function becomes negative; in view of this, $\mu_e \approx \mu$. The correct prediction of effective viscosity in the laminar and fully turbulent region of flow makes possible the use of the RNG-model for calculating transition modes of flow.

The filter width Δ is related to the size of step of difference grid, $\Delta = V^{1/3}$, where V is the cell volume.

The inclusion of compressibility in the subgrid-scale model affects the results of numerical simulation only slightly [21]

INITIAL AND BOUNDARY CONDITIONS

In the case of large eddy simulation, unsteady-state boundary conditions defined by the fluctuation pattern of flow need to be assigned in the inlet section. Free shear flows are unstable, and oscillation in these flows arises in the absence of external sources of disturbances [12].

Correct assignment of boundary conditions calls for the calculation of flow in the pipe and in the boundary layer on the external surface of the nozzle [14] (a part of the nozzle is included in the computational domain). In view of the laboriousness of this problem, no calculation of flow in pipe is performed, and a velocity profile is preassigned at the nozzle exit section (at $|r| \le r_a$), on which random sine disturbances are superimposed [18],

$$v_x(r, t) = \frac{u_a}{3}\left[1 + \tanh\left(\frac{0.5 - |r|}{2\delta}\right)\right][1 + \alpha\sin(\mathrm{Sh})],$$

where δ is the momentum thickness, α is the amplitude of disturbances, and Sh is the Strouhal number. It is assumed in the calculations that $\delta/r_a \sim 0.1$, $\alpha = 2.1 \times 10^{-3}$, and Sh = 0.42. Small random disturbances are further superimposed on the radial distribution of circumferential velocity

$$v_\theta(r, t) = 0.025\exp[-3(1 - |r|)^2]\xi,$$

where ξ is a random number from uniform distribution in the [–0.5, 0.5] interval. The radial velocity at the nozzle exit section is taken to be zero.

The boundary conditions away from a jet flowing out into submerged space are defined by the ejection properties of the jet: an induced potential flow directed toward the jet exists away from the jet. The properties and parameters of this flow are not known in advance and are defined by the jet proper. The calculations of steady-state flows reveal that the best results are produced by the boundary conditions based on exact solution which describes a potential flow outside of a round turbulent jet [12].

Nonreflecting boundary conditions are used for sought variables on the boundaries across which the gas leaves the computational domain.

NUMERICAL METHOD

The quantization of Eq. (1) is performed using the control volume approach [22]. The third-order Runge-Kutta method is used for quantization of time derivatives. The flow vector is split into the nonviscous and viscous components. The method of piecewise-parabolic reconstruction and the Chakrawarthy–Osher scheme are used for quantization of nonviscous flows, and second-order centered finite-difference formulas – for quantization of viscous flows. The set of difference equations is solved by multigrid method using a complete approximation scheme.

The computational procedure involves computer codes in FORTRAN and C/C++. The message passing interface (MPI) is used for deparallelizing the computational procedure.

The calculations were performed in an IBM SP/1600 supercomputer (eServer pSeries 690, Power 4+ 1.7 GHz processor). The supercomputer center is located at the Central Laboratory of the Research Council (Daresbury Laboratory, Warrington, United Kingdom).

CALCULATION RESULTS

The following values were assigned to the parameters of the problem: $r_a = 5$ mm, $u_a = 80$ m/s, $\rho_a = 0.58$–1.26 kg/m^3, $T_a = 280$–600 K, $\rho_\infty = 0.58$–1.26 kg/m^3, and $T_\infty = 280$–600 K. The parameters at the nozzle exit section correspond to Reynolds number $\mathrm{Re} = 1.2 \times 10^5$, which is maintained constant owing to proper variation of dynamic viscosity, and to the range of variation of degree of preheating $\varphi = 0.48$–2.15.

The calculations are performed in the range $[0, L_x] \times [-L_y, L_y] \times [-L_z, L_z]$. The length of computational

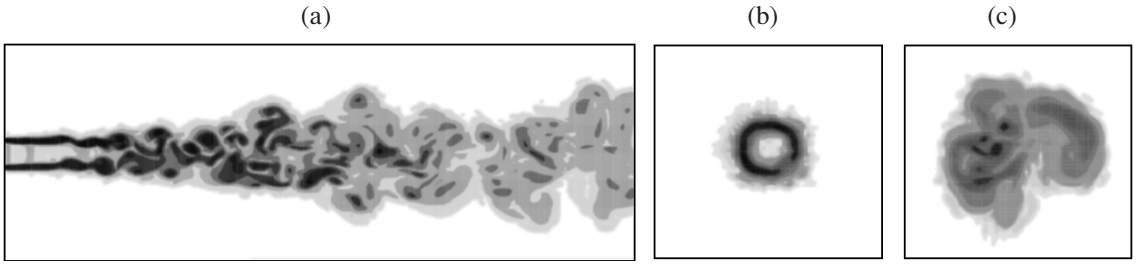

Fig. 1. The level lines of vorticity at instant of time $t = 2.32$ s in (a) the middle section of the jet, (b) $x/r_a = 10$ sections, and (c) $x/r_a = 80$.

domain is $L_x = 100r_a$, and its width and height in the inlet and outlet sections are $L_y = L_z = 10r_a$ and $L_y = L_z = 40r_a$.

The grid has $350 \times 150 \times 150 = 7\,875\,000$ cells. In the initial region of the jet, the step for variable x is taken to be constant until the section of $x \sim 10r_a$ and then increases gradually by the law of geometric progression. In the cross section, the grid nodes are crowding towards the nozzle edges. The steps in coordinate directions have the following values: $\Delta x_{\min} = 0.08r_a$, $\Delta x_{\max} = 0.15r_a$, $\Delta y_{\min} = \Delta z_{\min} = 0.03r_a$, and $\Delta y_{\max} = \Delta z_{\max} = 0.09r_a$. The time step is $\Delta t = 0.08r_a/u_a = 5.8 \times 10^{-5}$ s. A statistically reliable averaged pattern of flow is obtained by making 10^5 time steps.

The vorticity $\Omega = |\nabla \times \mathbf{v}|$ is used for visualizing the instantaneous pattern of flow in the jet.

Level lines of vorticity are given in Fig. 1 at $\varphi = 1.2$. Large-scale eddy structures are present in the shear layer of the jet in the form of toroidal axisymmetric eddies arising at some distance from the nozzle exit section (approximately one or two diameters). In the initial region of the jet, the characteristic size of eddy structures is fairly small. Downstream of the initial region, the characteristic size of eddy structures increases, and the momentum exchange between the jet and surrounding liquid is intensified. The contours of coherent structure are ellipses, this implying the anisotropy of turbulent pulsations. The generation of eddies is associated with the Kelvin–Helmholtz instability of the shear layer. The maxima and minima of vorticity approximately correspond to the centers of eddies.

The calculation results demonstrate that the velocity and temperature profiles in the flow cross section exhibit a typical jet pattern, as well as a kink in the middle part. The profiles become wider with increasing coordinate x, which points to the increase in the thickness of the zone of jet with the ambient medium. In the vicinity of the jet boundary, the profiles of sought characteristics of flow become gently sloping.

As a result of the impact made by nonisothermality on the turbulent structure of the jet, the maximal value of intensity of fluctuations of longitudinal velocity at $\varphi < 2.1$ increases with the degree of preheating and amounts to about 25% of velocity at the nozzle exit section (Fig. 2). This is much higher than the respective values in a jet of cold gas, where they do not exceed 16% [8, 9].

As the degree of preheating of the jet increases, the maximum of fluctuations of longitudinal velocity shifts toward the nozzle exit section. A further increase in the degree of preheating causes a qualitative variation of the pattern of this impact (according to the data of Gorshkov [9]); as a result, the maximum of fluctuations of longitudinal velocity decreases. A similar impact is made by the nonisothermality of flow on the distribution of intensity of temperature fluctuations, the maxi-

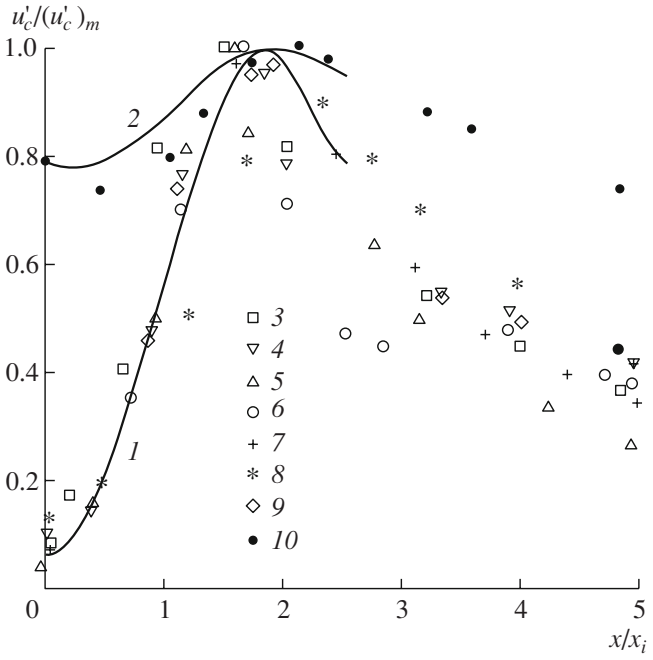

Fig. 2. The distribution of intensity of turbulence along axial coordinate. Curves *1* and *2* correspond to the results of calculations for jets with natural ($\theta = 2\%$) and increased ($\theta = 8\%$) levels of turbulence at the nozzle exit section: (*3*) experimental data of [8] ($\varphi = 2.6$), (*4*) data of [8] ($\varphi = 3.9$), (*5*) [8] ($\varphi = 5$), (*6*) [6] ($\varphi = 2$), (*7*) [9] ($\varphi = 1$, $\theta = 1.5\%$), (*8*) [7] ($\varphi = 2.32$, $\theta = 1.5\%$), (*9*) [1] ($\varphi = 1$, $\theta = 9.3\%$), (*10*) [1] ($\varphi = 1$, $\theta = 20.9\%$).

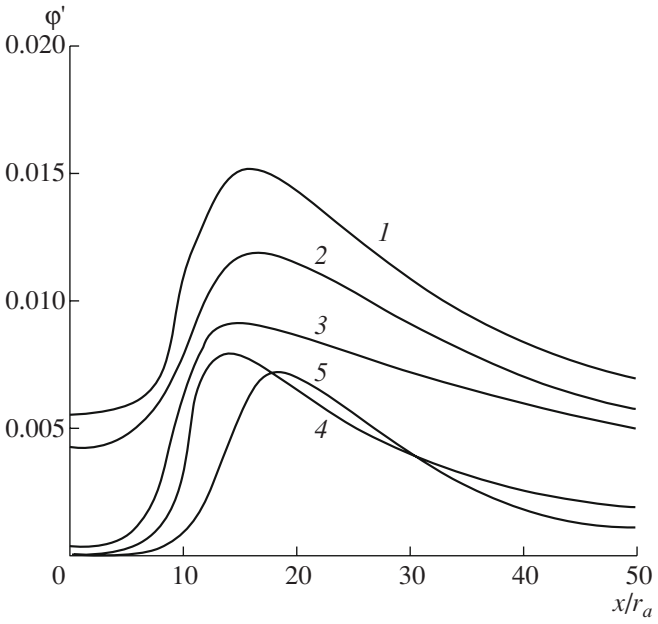

Fig. 3. The distribution of mean-square values of fluctuations of (*1*) axial velocity, (*2*) radial velocity, (*3*) temperature, and (*4*) correlation moment of fluctuations of axial velocity and temperature along the jet axis at φ = 1.2. Curve *5* corresponds to the data of [5].

mal value of which is of the order of 13% of the temperature difference at the nozzle exit section.

The results of [1, 7, 9] demonstrate that the maximal values of fluctuations of longitudinal velocity occur at $x/r_a \sim 16$. In the region of core of constant velocity, the intensity of turbulence, while remaining almost constant in the transverse direction, increases from 1.5–2% at the nozzle exit section to a value of the order of 6% at the end of the initial region with increasing distance from the nozzle exit section. Because no turbulent mixing is present within the core, the effect of the increase in the degree of turbulence is associated with the penetration of pressure fluctuations from the mixing zone into the core. The fluctuations of velocity on the jet axis reach a maximal value at a distance equal to two lengths of initial segment x_i (Fig. 2, subscript *c* indicates the jet axis). This value remains almost constant for both isothermal and nonisothermal jets and depends relatively weakly on the conditions of outflow [9].

The increase in the level of turbulence at the nozzle exit section (at θ > 5%) causes the rearrangement of the microstructure of flow, the intensification of the mixing of jet with surrounding gas, and the decrease in the range of the jet [1] (down to complete disappearance of the initial segment). A significant difference is observed in the pattern of variation of kinetic turbulent energy along the jet axis at low and high levels of initial turbulence. At a low degree of turbulence at the nozzle exit section, the kinetic turbulent energy first increases, reaches a maximum, and then slowly decreases. In the case of a high level of turbulence at the nozzle exit section, the kinetic turbulent energy first decreases abruptly along the jet axis, after which it starts increasing and reaches a maximum; then it decreases downstream by the power law. At very high values of the initial degree of turbulence, the kinetic turbulent energy continuously decreases downstream.

Figure 3 gives the distribution of mean-square values of fluctuations of axial velocity $\langle v_x'^2 \rangle$, radial velocity $\langle v_r'^2 \rangle$, and temperature $\langle T'^2 \rangle$, as well as of the product correlation moment of fluctuations of axial velocity and temperature $\langle v_x' T' \rangle$ along longitudinal coordinate. Curve *5* from [5] corresponds to the approximate solution by the model of [10]. The calculation results are normalized to $10u_a$ and the temperature difference of $10\Delta T_a$. In the initial segment of the jet, the fluctuation parameters assume values typical of fully developed turbulent flow in a round pipe. In the far field of jet flow, these values vary by a close-to-power law. The increase in temperature fluctuations begins from a distance $x/r_a \sim 6$, while the fluctuations of longitudinal and radial velocity start increasing at $x/r_a \sim 8$. These values of longitudinal coordinate, which correspond to the lengths of the thermal and dynamic initial regions, are close to values corresponding to the minima of distributions of skewness and flatness factors of temperature and velocity.

The distributions of fluctuations of axial velocity and temperature $\langle v_x' T' \rangle$ and fluctuations of radial velocity and temperature $\langle v_r' T' \rangle$ in the jet cross section are given in Fig. 4. Radial coordinate is normalized to the half radius of the jet r_u. The data of [2] correspond to cross section $x/r_a = 118$, and the data of [3, 4]—to cross section $x/r_a = 30$.

The values of radial coordinate, at which the correlation moments of velocity and temperature reach a maximal value, almost coincide in cross sections $x/r_a = 10$ and $x/r_a = 30$ and correspond to the position of maximum of kinetic turbulent energy ($r/r_u = 0.8$ according to the data of [3] and $r/r_u = 0.7$ according to the data of [4]). However, the maximal value and shape of the calculated profiles, especially, of the product moment of fluctuations of axial velocity and temperature, differ from those obtained experimentally. Apparently, this is explained by the impact of the conditions at the nozzle exit section. The calculation results for the moment $\langle v_r' T' \rangle$ better agree with the measurement data than those for the moment $\langle v_x' T' \rangle$.

In the near field of jet flow (at $x/r_a \sim 10$), the heat transfer occurs along axial coordinate, because $\langle v_x' T' \rangle / \langle v_r' T' \rangle \sim 2$ in the $0.2 < r/r_u < 1.4$ range. Downstream (at $x/r_a \sim 30$), the contributions made by the longitudinal and radial heat fluxes become approximately

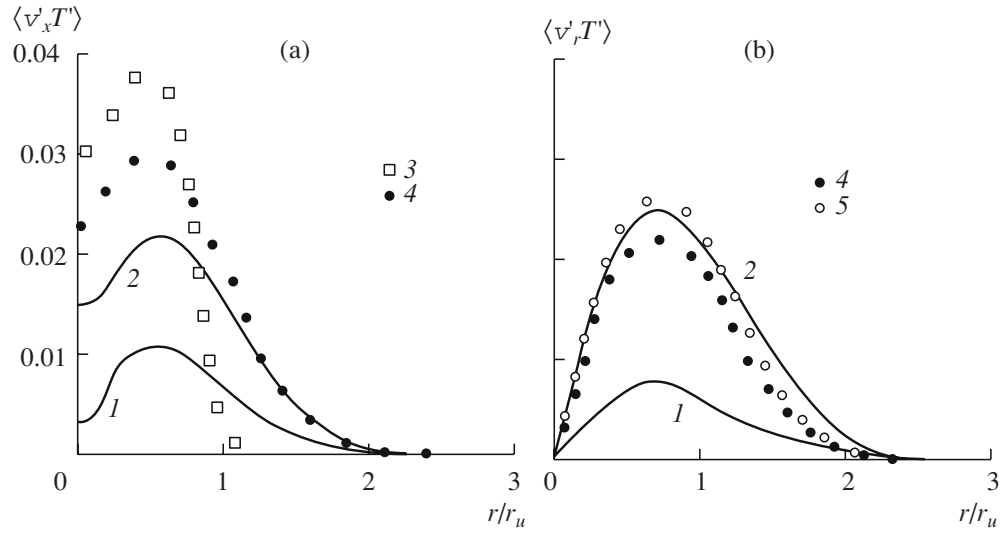

Fig. 4. The distribution of the product correlation moments of fluctuations of (a) axial velocity and temperature and (b) radial velocity and temperature at φ = 1.2 in cross sections (*1*) $x/r_a = 10$ and (*2*) $x/r_a = 30$ compared to the data of (*3*) [2], (*4*) [3], and (*5*) [4].

equal, so that $\langle v_x' T' \rangle / \langle v_r' T' \rangle \sim 1.1$ in the $0.5 < r/r_u < 1.8$ range. Note that, in a plane jet, $\langle v_x' T' \rangle / \langle v_r' T' \rangle \sim 2$ at $x/r_a = 80$ and in the range of variation of radial coordinate of $0.4 < r/r_u < 1.3$ [2] (at $\mathrm{Re} = 7.9 \times 10^3$ and $\Delta T_a = 25$ K). In an axisymmetric jet, the measurements of Antonia et al. [2] give $\langle v_x' T' \rangle / \langle v_r' T' \rangle \sim 1$ downstream of cross section $x/r_a \sim 100$ and in the range of $0.3 < r/r_u < 1.3$.

The distributions of correlation moments of fluctuations of density and velocity along the jet axis, which characterize the anisotropy of mass flow, are given in Fig. 5 for two values of the degree of preheating (calculations are normalized to $\rho_a u_a$). The calculation results are in qualitative agreement with the data of Gazzah et al. [11] obtained using the k–ε model of turbulence which does not include the anisotropy of turbulent fluctuations of velocity but enables one to estimate the anisotropy of diffusion flow of mass. The anisotropy is observed in the middle of the jet at $4 < x/r_a < 40$. Downstream, we have $\langle \rho' v_r' \rangle / \langle \rho' v_x' \rangle \sim 1$ (at $x/r_a > 40$).

The difference of distribution of probability of fluctuations of function φ from Gaussian distribution is characterized by the skewness factor S_φ (third moment) and flatness factor F_φ (fourth moment). The coefficient of nth moment is found from the relation $M_n(\varphi) = \langle \varphi'^n \rangle / \langle \varphi'^2 \rangle^{n/2}$. In so doing, $S_\varphi = M_3$ ($n = 3$) and $F_\varphi = M_4$ ($n = 4$). For normal distribution of probability, $S_\varphi = 0$ and $F_\varphi = 3$.

The obtained results demonstrate that the distributions of skewness and flatness factors along the jet axis are nonmonotonic. At small distances from the nozzle exit section (at $x/r_a < 6$), the fluctuations of velocity and temperature approximately satisfy the normal probability distribution, which is reflective of the respective normal distribution of velocity and temperature fluctuations at the nozzle exit section. High values of the skewness and flatness factors are observed at the end of potential core. At $x/r_a > 40$, non-Gaussian probability distribution is observed.

The longitudinal distributions of the skewness and flatness factors of the field of velocity and temperature are given in Fig. 6. While the distributions of the third

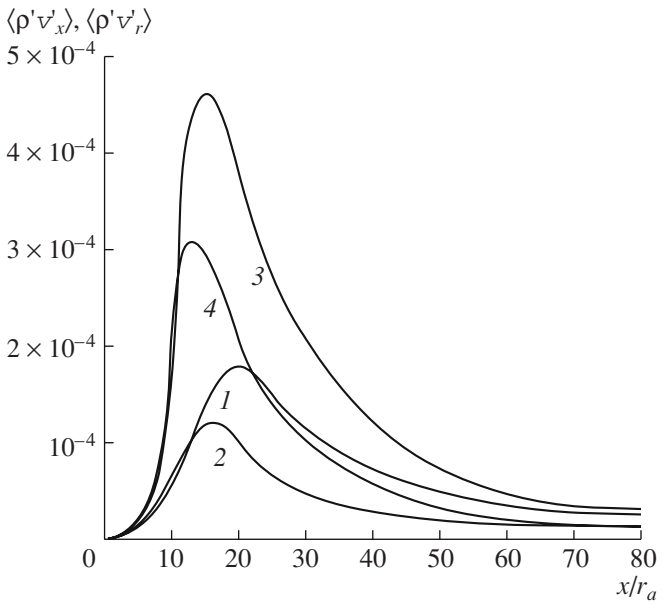

Fig. 5. The distribution of moments (*1*, *3*) $\langle \rho' v_x' \rangle$ and (*2*, *4*) $\langle \rho' v_r' \rangle$ along the jet axis at (*1*, *2*) φ = 0.6 and (*3*, *4*) φ = 2.

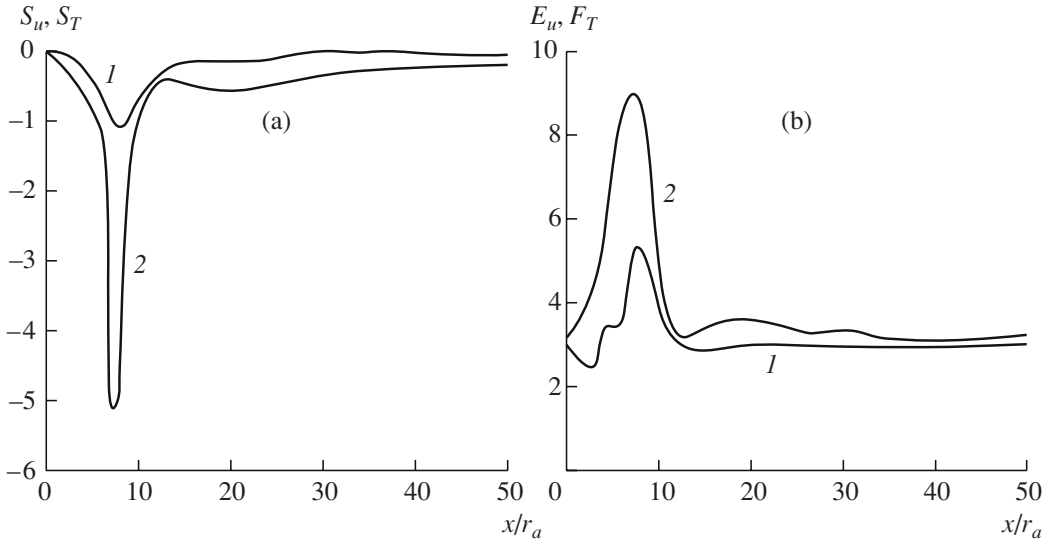

Fig. 6. The distributions of (a) skewness and (b) flatness factors of fluctuations of (*1*) velocity and (*2*) temperature along the jet axis at φ = 1.2.

and fourth moments of fluctuations of velocity and temperature are qualitatively and quantitatively similar in the far flow of the jet, they significantly differ in behavior at $0.4 < x/r_a < 16$. The rearrangement of S_T and F_T distributions is faster than that of S_v and F_v; in particular, the factors S_T and F_T reach maximal values at $x/r_a \sim 6$, while S_v and F_v—at $x/r_a \sim 10$. Their maximum corresponds to the jet section in which the mixing layers reach the jet axis. In so doing, the maximal values of S_T and F_T significantly exceed the respective values for the velocity field. Similar tendencies are observed in [5], where $S_T \sim 8$ at $x/r_a \sim 8$ for a plane jet. The minimal value of the correlation factor of longitudinal velocity and temperature is 0.2 and is reached in the same section where the maxima of S_T and F_T are observed (at $x/r_a \sim 6$). In the far field of jet flow, the S_v and F_v distributions are described by Gaussian curve; in so doing, $S_T \sim -0.5$ and $F_T \sim 3.3$.

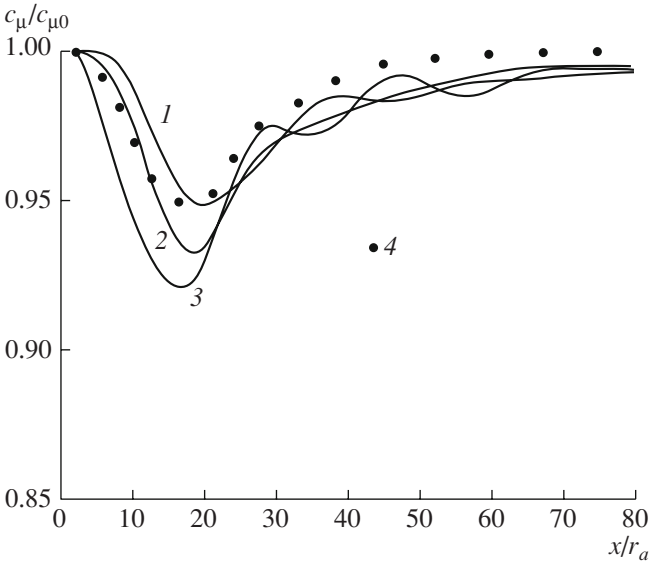

Fig. 7. The variation of constant c_μ appearing in the formula for turbulent viscosity along the jet axis at φ = (*1*) 0.6, (*2*) 1, and (*3*) 1.8; (*4*) corresponds to the correlation in [10].

The density of distribution of probability of velocity fluctuations exhibits a symmetric shape which is close to Gaussian at $x/r_a \sim 10$. The density of distribution of probability of temperature fluctuations differs from Gaussian. At $x/r_a \sim 30$, their qualitative behavior does not vary; however, the skewness (asymmetry) of distribution of probability of temperature fluctuations becomes appreciable.

The distributions of constants appearing in the basic relations (for example, constant c_μ in the formula for turbulent viscosity and turbulent Prandtl number) are of great importance from the standpoint of verifying the calculation results obtained using the Reynolds-averaged Navier–Stokes equations and the *k*–ε model of turbulence.

The data of physical experiment (flows in pipes and in boundary layers) demonstrate that the surface friction stress turns out to be proportional to the kinetic turbulent energy (the so-called Nevzglyadov–Dryden hypothesis) with the proportionality factor confined in a rather narrow range. This substantiates the assignment of the relevant value to the coefficient appearing in the formula for turbulent viscosity.

The variation of constant in the *k*–ε model of turbulence along the jet axis for different values of degree of preheating is shown in Fig. 7. The calculation results are normalized to the "standard" value of constant $c_{\mu 0} = 0.09$. The maximal deviation from the "standard" value

is observed in the $12 < x/r_a < 20$ range and exhibits a tendency to shifting toward the nozzle exit section with increasing degree of preheating of the jet. The deviation from the standard value is 5.2% at $\varphi = 0.6$, 6.2% at $\varphi = 1$, and 7.9% at $\varphi = 1.8$.

The results obtained for isothermal jet agree quite well with the correlation of [10] (the so-called k–ε1 model of turbulence),

$$c_\mu = 0.09 - 0.04f, \quad f = \left|\frac{\delta}{2\Delta U}\left(\frac{dU_c}{dx} - \left|\frac{dU_c}{dx}\right|\right)\right|,$$

where δ is the mixing zone thickness, and ΔU is the characteristic variation of velocity in the mixing layer. The major differences are observed in the far field of jet flow, where the calculations produce lower values of the constant. The minimal value of the constant is likewise lower than the value obtained by the data of [10].

The turbulent Prandtl number is calculated by the formula

$$\mathrm{Pr}_t = \langle v_x' v_r' \rangle \frac{\partial \langle T \rangle}{\partial r}\left(\langle v_r' T' \rangle \frac{\partial \langle v_x \rangle}{\partial r}\right)^{-1}.$$

The l'Hospital rule is employed on the jet axis for overcoming the indeterminacy.

The distributions of turbulent Prandtl number in cross sections of a jet are given in Fig. 8. The maximal values of Prandtl number are attained on the jet axis. In the far field of jet flow, the Prandtl number varies relatively slightly. The minimal value of Prandtl number is attained at $r/r_u \sim 0.62$ and exhibits a weak dependence on the parameters at the nozzle exit section. When r/r_u varies from zero to 0.6, the value of turbulent Prandtl number decreases by a factor of almost three (from 1.5 on the jet axis to 0.5 in the mixing layer).

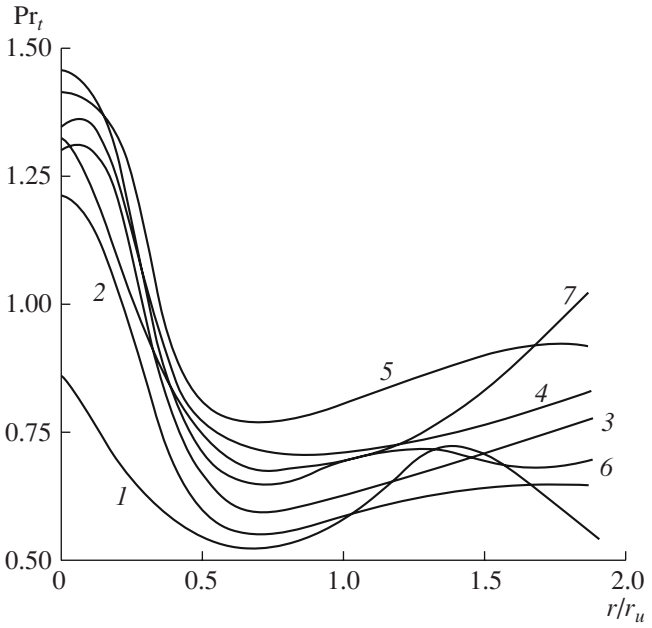

Fig. 8. The distribution of turbulent Prandtl number in cross sections of the jet at $\varphi = 1.6$ and x/r_a = (*1*) 10, (*2*) 14, (*3*) 16, (*4*) 18, (*5*) 24, (*6*) 28, and (*7*) 80.

CONCLUSIONS

Large eddy simulation was performed in a nonisothermal jet flowing out from a round nozzle into submerged space at different values of the degree of preheating and of the level of turbulence at the nozzle exit section. The distributions of correlation moments of fluctuations of density, velocity, and temperature, including those of higher-order moments, as well as the distributions of turbulent Prandtl number and of the constant which appears in the formula for turbulent viscosity, were obtained along the axis and in cross sections of jet flow. The calculation results are in qualitative and quantitative agreement with the known characteristics of propagation of isothermal and nonisothermal jets.

The increase in the degree of preheating of the jet causes a reduction of the length of initial section and an increase in the degree of expansion of the jet; the damping of the gasdynamic, thermal, and fluctuation parameters in the region of jet expansion is more intensive than that in the case of isothermal jet or jet with a lower degree of preheating. Nevertheless, the preheating of the jet does not cause significant qualitative changes of the microstructure of submerged jets. The maximal value of fluctuations of longitudinal velocity in the zone of mixing of the jet is of the order of 15–17% of the gas velocity at the nozzle exit section. The maximum of fluctuations of longitudinal velocity on the jet axis is located at a distance approximately equal to two lengths of initial section and is of the order of 13–15% of the respective value for cold jets. The radial distribution of velocity fluctuations in the mixing zone is characterized by a maximum shifting toward the jet axis away from the nozzle exit section.

REFERENCES

1. Ginevskii, A.S., *Teoriya turbulentnykh strui i sledov* (The Theory of Turbulent Jets and Traces), Moscow: Mashinostroenie, 1969.
2. Antonia, R.A., Prabhu, A., and Stephenson, S.E., *J. Fluid Mech.*, 1975, vol. 72, no. 3, p. 455.
3. Chevray, R. and Tutu, N.K., *J. Fluid Mech.*, 1978, vol. 88, no. 1, p. 133.
4. Chua, L.P. and Antonia, R.A., *Int. J. Heat Mass Transfer*, 1990, vol. 33, no. 2, p. 331.
5. Pietri, L., Amielh, M., and Anselmet, F., *Int. J. Heat Fluid Flow*, 2000, vol. 21, p. 22.
6. Kukes, V.I. and Yarin, L.P., Investigation of Turbulent Heat Transfer in Nonisothermal Jets, in *Materialy V Vsesoyuznoi konferentsii po teplomassoobmenu* (Proceedings of V All-Union Conference on Heat and Mass

Transfer), Minsk: Izd. ITMO AN BSSR, 1976, vol. 1, p. 167.

7. Lau, J.C., *J. Fluid Mech.*, 1981, vol. 105, p. 193.
8. Ustimenko, B.P., Zmeikov, V.N., Shishkin, A.A., and Rivin, B.O., The Effect of the Degree of Nonisothermality of Flow on the Characteristics of Jet Flow, in *Turbulentnye struinye techeniya* (Turbulent Jet Flows), Tallinn: Izd. ITEF AN ESSR, 1985, p. 21.
9. Gorshkov, G.F., Propagation of Cocurrent Nonisothermal Jets of Gas and Plasma of Varying Composition, in *Dinamika neodnorodnykh i szhimaemykh sred* (The Dynamics of Inhomogeneous and Compressible Media), Leningrad: Izd. LGU (Leningrad State Univ.), 1984, p. 164.
10. Launder, B.E., Morse, A., Rodi, W., and Spalding, D.B., Prediction of Free Shear Flows. A Comparison of the Performance of Six Turbulence Models, *Free Turbulent Shear Flows. NASA Report*, 1973, no. SP-321.
11. Gazzah, M.H., Sassi, M., Sarh, B., and Gokalp, I., *Int. J. Therm. Sci*, 2002, vol. 41, p. 51.
12. Lyubimov, D.A., *Aeromekh. Gaz. Din.*, 2003, no. 3, p. 14.
13. Shur, M.L., Spalart, P.R., Strelets, M.Kh., and Travin, A.K., *Int. J. Heat Fluid Flow*, 2003, vol. 24, p. 551.
14. Tucker, P.G., *Int. J. Heat Fluid Flow*, 2004, vol. 25, p. 625.
15. Yan, H. and Su, M., *Commun. Nonlinear Sci. Numer. Simul.*, 1999, vol. 4, no. 1, p. 12.
16. Ilyushin, B.B. and Krasinskii, D.V., *Teplofiz. Aeromekh.*, 2006, vol. 13, no. 1, p. 49.
17. Salinas-Vazquez, M., Vicente, W., Espinosa, A., and Barrios, E., *Am. J. Appl. Sci.*, 2005, vol. 2, no. 8, p. 1270.
18. Boersma, B.J. and Lele, S.K., Large Eddy Simulation of Compressible Turbulent Jets, *Center for Turbulence Research. Annual Research Brief*, 1999, p. 365.
19. Yakhot, A., Orszag, S.A., Yakhot, V., and Israeli, M., *J. Sci. Comput.*, 1986, vol. 1, p. 1.
20. Smagorinsky, J., *Mon. Weather Rev.*, 1963, vol. 91, no. 3, p. 99.
21. Martin, M.P., Piomelli, U., and Candler, G.V., *Theor. Comput. Fluid Dyn.*, 2000, vol. 13, p. 361.
22. Volkov, K.N., *Vychisl. Metody Program.*, 2005, vol. 6, no. 1, p. 43.